Molecular Dynamics Simulations of Adsorption of Amino Acid Side Chain Analogs and a Titanium Binding Peptide on the TiO 2 (100) Surface

ARTICLE *in* THE JOURNAL OF PHYSICAL CHEMISTRY C · AUGUST 2015

Impact Factor: 4.77 · DOI: 10.1021/acs.jpcc.5b02670

2 AUTHORS, INCLUDING:

Alexander P Lyubartsev
Stockholm University
155 PUBLICATIONS **4,766** CITATIONS

THE JOURNAL OF PHYSICAL CHEMISTRY C

Article

pubs.acs.org/JPCC

Molecular Dynamics Simulations of Adsorption of Amino Acid Side Chain Analogues and a Titanium Binding Peptide on the TiO_2 (100) Surface

Erik G. Brandt and Alexander P. Lyubartsev*

Department of Materials and Environmental Chemistry, Stockholm University, SE-106 91, Stockholm, Sweden

ABSTRACT: Adsorption profiles and adsorption free energies were determined for the side chain analogues of the 20 naturally occurring amino acids and a titanium binding peptide on the TiO_2 (100) surface. Microsecond simulations with umbrella sampling and metadynamics were used to sample the free energy barriers associated with desolvation of strongly bound water molecules at the TiO_2 surface. Polar and aromatic side chain analogues that hydrogen bond either to surface waters or directly to the metal oxide surface were found to be the strongest binders. Further, adsorption simulations of a 6-residue titanium binding peptide identified two binding modes on TiO_2 (100). The peptide structure with lowest free energy was shown to be stabilized by a salt bridge between the end termini. A comparison between the free energies of the side chain analogues of the peptide sequence and the peptide itself shows that the free energy contributions are not additive. The simulations emphasize that tightly bound surface waters play a key role for peptide and protein structures when bound to inorganic surfaces in biological environments.

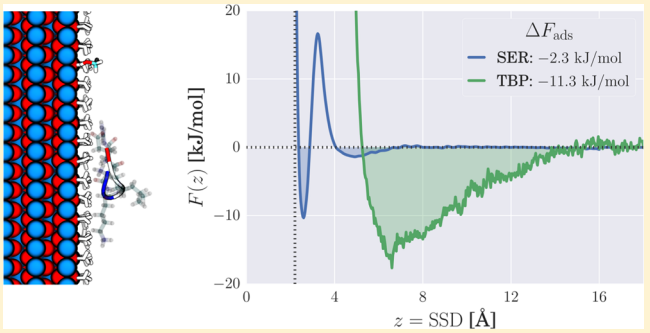

INTRODUCTION

Inorganic materials in biological environments attract proteins and other biomolecules that adsorb on the material surface.[1] Understanding the molecular interactions at this nanobio interface is of key importance in applications such as safe medical implants,[2] protein corona formation and its role in nanotoxicity,[3] the efficiency of biosensor surfaces,[4] and many others. Materials containing titanium (Ti) are often found in biological milieus, e.g., in medical implants[5] and consumer products.[6] Titanium surfaces are oxidized under ambient conditions, which effectively leads to titanium dioxide surfaces being exposed into the environment. TiO_2 is also present in biological organisms in form of engineered nanoparticles (NPs), either by intentional use (cosmetics), or due to uptake from the environment. Understanding the interactions between TiO_2 and biomolecules could potentially improve the design of safe nanomaterials and increase the efficiency of nanomedicine.[7]

The 6-residue peptide with sequence RKLPDA[8] is an important case for modeling TiO_2−biomolecule interactions, since it has been shown to bind selectively to metal surfaces (to Ti, Si and Ag but not to, e.g., Au, Pt, and Zn[9]). NMR experiments have revealed that the peptide binds to TiO_2 in a compact, "C"-shaped, structure, which was suggested to result from electrostatic interactions between the peptide termini and the metal oxide surface.[10] Experimental techniques such as phage selection and NMR can be used to determine the peptide sequence and ensemble structure, but does not provide a direct view of the molecular motions during adsorption.

However, molecular simulations can be used as "virtual microscopes" to study adsorption on inorganic surfaces in atomistic detail.[11] Simulations have been used to identify binding modes,[12] calculate adsorption free energies,[13] and studying protein unfolding kinetics.[14] Atomistic simulations of biomolecular adsorption on inorganic surfaces are impeded by two main factors. First, unified descriptions for simulations of inorganic surfaces and biomolecules are still underdeveloped, and this is an active area of research.[15] Second, atomistic simulations can access time scales up to 1 μs, but modeling adsorption on polar surfaces can require significantly longer simulation times.

The first problem is addressed by us in an accompanying paper[16] where the aim is to develop robust force field parameters for interactions between TiO_2 surfaces and biomolecules. The present work is focused on the second problem: to enhance sampling in atomistic simulations of biomolecular adsorption on TiO_2 surfaces, with the aim to calculate accurate adsorption profiles and adsorption free energies. In conventional simulations, biomolecules stay adsorbed to the polar material surface for the entire simulation time, and reversible binding/unbinding of even small polypeptides is not observed. The adsorbate stays trapped to the surface in whatever configuration it first happened to bind. In short, the statistical sampling in conventional simulations is

Received: March 19, 2015
Revised: June 27, 2015
Published: July 16, 2015

DOI: 10.1021/acs.jpcc.5b02670
J. Phys. Chem. C 2015, 119, 18126−18139

incomplete. The TiO_2−water interface dynamics is further complicated by tightly bound surface waters with which the adsorbate must compete to gain access to the metal oxide surface. Penetrating the solvation layer may involve a free energy barrier of as much as 12 k_BT.[16]

We use molecular dynamics (MD) with two enhanced sampling methods to overcome the sampling problem and calculate the adsorption profiles (potentials of mean force) and adsorption free energies for amino acid side chain analogues (SCAs) on TiO_2 (100). Within the ideal adsorbed solution theory, these free energy profiles can be used as effective potentials in coarse-grained models of protein−surface interactions. Previous MD simulations of SCAs[17] and the RKLPDA-peptide[18] have been performed on the (110) surface,[17] which consists of protruding oxygens ("bridging rails") on a flat surface of Ti−O atoms. The oxygen-terminated (100) surface employed in this work is probably a more accurate description of titanium surfaces in aqueous media, which are expected to be oxygen-covered under ambient conditions (neutral pH and biological salt concentration),[19−21] e.g., as implants[22] or nanoparticle surfaces. The adsorption free energies for the side chain analogues provide a map of the interactions underlying protein adsorption on TiO_2, and serve to further predict adsorption of larger proteins to TiO_2 surfaces.

Furthermore, the adsorption of the peptide sequence RKLPDA on TiO_2 (100) was investigated using both unbiased and biased molecular dynamics simulations, and analyzed using free energy landscapes obtained with enhanced sampling. The present simulation results confirm previous work[23] focused on finding the peptide's Ti/Si-selection mechanism between oxidized titanium and silicon surfaces, and accentuate the important role of the surface solvation layer in understanding protein adsorption on polar surfaces. In all, the present work extends previous simulation efforts with an order of magnitude in terms of sampling times.

The "Theory" section covers the chemical theory of adsorption, how free energies are calculated from simulations, and how the adsorbed molecular orientation can be analyzed in terms of Euler angles. The "Materials and Methods" section describes the systems and the simulation protocols used in the calculations. The "Results" section reports the simulation results and the analysis of the adsorption profiles for the side chain analogues and the peptide. The adsorption of the titanium binding peptide is described in terms of a two-dimensional free energy landscape. The "Conclusions" section summarizes the most important insights from this work with directions for future work.

THEORY

Surface Adsorption Free Energy. The adsorption of a molecule on a solid surface is characterized by the free energy difference,

$$\Delta F_{ads} = F_{bound} - F_{free} \tag{1}$$

where F_{bound} and F_{free} denote the respective free energies associated with the molecule being bound to the surface, and the molecule being positioned far away where surface interactions are negligible. ΔF_{ads} is related to the (dimensionless) equilibrium constant of adsorption, K, by $\Delta F_{ads} = -k_BT \ln K$. Since the free energy is a state function, ΔF_{ads} is independent of the path the system takes between the bound and free configurations; it only depends on the free energy difference of the path's end points. Denoting the reaction coordinate by z, the probability of the system being in *any* state along z is given by the Boltzmann distribution,

$$P(z) = \frac{1}{Z} e^{-F(z)/k_BT}, \quad Z = \int_{-\infty}^{\infty} dz e^{-F(z)/k_BT} \tag{2}$$

with the partition function Z acting as the normalization factor. (The direct calculation of Z from a simulation is a great challenge and is usually circumvented). Subsequently, the probability of the molecule being in the bound state is

$$P_{bound} = e^{-F_{bound}/k_BT} = \frac{\int_{-\infty}^{\infty} dz I_{bound}(z) P(z)}{\int_{-\infty}^{\infty} dz I_{bound}(z)} \tag{3}$$

with an analogous equation defining P_{free}. $I_{bound}(z)$ and its counterpart $I_{free}(z)$ are indicator functions that are nonzero only for values of z where the molecule is bound (or free, for the opposite case). The region of the bound state is defined (with some degree of arbitrariness) from the distance of the closest approach of the molecule to the surface (r_c) to the point where the solvent can be considered as bulk (usually taken at point where the potential of mean force reaches the bulk value, $r_c + \delta$):

$$I_{bound}(z) = \begin{cases} 1 & r_c \le z \le r_c + \delta \\ 0 & \text{otherwise} \end{cases} \tag{4}$$

$$I_{free}(z) = \begin{cases} 1 & r_c + \delta < z < z_{max} \\ 0 & \text{otherwise} \end{cases} \tag{5}$$

Free energy (as well as probability) of the free state depends on the volume of the free state defined by z_{max} in eq 5. Usually a reference state is defined which corresponds to the solute concentration 1 M in the case of "standard free energy". We define the reference free state to have the same volume as the bound state; that is, the indicator function $I_{free}(z)$ is equal to 1 in a range of z corresponding to bulk solution and having length δ (i.e., $z_{max} = r_c + 2\,\delta$ in eq5). It is easy, however, to recalculate the free energy to any other "standard" state by adding the term $k_BT \ln(c/c_{st})$ to the calculated free energy, where c and c_{st} are the concentration of the substance in the simulation and in the other standard state, respectively. The above considerations lead to the definition of the binding free energy in terms of the excess free energy. Shifting the adsorption profile (potential of mean force) to be zero in the bulk region ($F(z) = 0$ for $z \ge r_c + \delta$) we have finally from eqs 1−5:

$$\Delta F_{ads} = -k_BT \ln\left(\frac{1}{\delta}\int_{r_c}^{r_c+\delta} dz e^{-F(z)/k_BT}\right) \tag{6}$$

for the adsorption free energy. Note in passing that Z has been canceled from the final expression. Admittedly, the limits of the bound regime is to some extent arbitrary, but note that the exponential in eq 6 is large for negative $F(z)$. The adsorption free energy is therefore insensitive to the exact starting position $z = r_c$, where $F(z)$ values are expected to be close to zero. Because of the δ in the denominator of eq 6, ΔF_{ads} has only a weak logarithmic dependence on the exact value of the end of the bound state, δ, provided that the free energy profile is flat beyond $z = r_c + \delta$. Equation 6 is thus a robust and direct measure of the adsorption free energy. A similar expression has been derived to interpret adsorption in SPR experimental data.[24]

DOI: 10.1021/acs.jpcc.5b02670
J. Phys. Chem. C 2015, 119, 18126−18139

Free Energy Calculations. Simulations are used to track atoms interacting via a potential function $V(x)$ by numerically solving the equations of motion. The integration provides instant atomic positions (and velocities), which can be used to obtain the free energy F of the reaction coordinate $z = z(x_i)$ from the statistical mechanical relation

$$F(z) = \frac{1}{Z}\int \mathrm{d}x\ \delta(z - z(x_i))\mathrm{e}^{-V(x)/k_\mathrm{B}T} \tag{7}$$

where $x \equiv (x_1, ..., x_n)$ are the atomic positions, and Z is the partition function. $F(z)$ is often called the potential of mean force. Equation 7 can be evaluated in various ways. The most straightforward way to estimate the free energy along the reaction coordinate is from the probability histogram P_z obtained by counting the times state z is occupied and then using the relation $F_z = -k_\mathrm{B}T \ln P_z$. In practice, this method is often inefficient and even useless because the time associated with the system visiting all available states can be enormously long. In such cases, the system must be forced to visit the states along the reaction coordinate, especially states that are separated by high free energy barriers. This needs to be done in such a way that the bias introduced by the force can be assessed and accounted for in the analysis. Two methods introducing biased, or enhanced, sampling are considered in this paper.

Umbrella Sampling. The standard way to perform biased simulations is umbrella sampling, which restricts the system to a set of points ("windows") along the reaction coordinate z. An independent simulation is carried out within each window with a harmonic biasing potential,

$$V_i(z) = \frac{1}{2}k(z - z_i^0)^2 \tag{8}$$

where z_i^0 is the restriction point for window i. A histogram (probability distribution) is collected for each window, and all histograms are combined with proper weighting.[25] The force constant, k, is chosen to get appropriate overlap between adjacent distributions.

Adaptive Well-Tempered Metadynamics. One drawback with umbrella sampling is the requirement of one simulation per window. Other methods can compute the free energy on-the-fly by applying a time-dependent bias. Metadynamics (MetaD) is one such sampling method, which has been actively used and developed during the past decade.[26] MetaD exists in many flavors; the heart of the method lies at its capability to estimate the free energy profile for a reaction coordinate z (also called collective variable, CV). MetaD is easily generalized to multiple collective variables. The method works by applying a time-dependent bias to the system's potential energy, forcing the system away from regions of CV space that have already been visited. Starting from time zero, the bias is evolved according to

$$\dot{V}(z, t) = \omega\ \mathrm{e}^{-V(z(t),t)/k_\mathrm{B}\Delta T}\ \exp\left[-\frac{(z - z(t))^2}{2\sigma^2(t)}\right] \tag{9}$$

with ω being the initial filling rate and ΔT being a temperature boost factor that determines an effective height of the free energy barriers which can be reached. Because of the continuously decreasing bias height during the simulation, the solution of eq 9 converges to the long-time limit[27]

$$F(z) = -\lim_{t\to\infty}\frac{\Delta T + T}{\Delta T}V(z, t) + \text{const.} \tag{10}$$

if $\sigma^2(t) = \sigma^2$ is independent of t. $F(z)$ is then the free energy associated with the collective variable z, and the constant on the right-hand side remains undetermined but is independent of z. Equation 9 and eq 10 constitute the well-tempered version of metadynamics (WT-MetaD),[27] with standard MetaD being recovered in the limit $\Delta T \to \infty$. In practice, the free energy is estimated by

$$F(z) \approx -(1 + T/\Delta T)V(z, t) = -\frac{V(z, t)}{1 - f^{-1}} \tag{11}$$

at a large but finite time t. The parameter $f = 1 + \Delta T/T$ is called the bias factor.

If a time-independent σ is used in eq 9, its value must be carefully determined by observing the magnitude of the z-fluctuations in an unbiased simulation. An appropriate σ-value for the WT-MetaD simulation is then determined by trial-and-error. $V(z,t)$ is not guaranteed to converge to the true free energy for a suboptimal choice of σ. The convergence can be made less sensitive to parameter choice by dynamically adapting the Gaussian widths to the local free energy landscape, which also optimizes the filling time. Time-dependent Gaussians can be implemented based on different measures. One choice is the mean-square displacement of z in a predetermined time window. In this approach, the Gaussian center and width at time t are exponentially weighted averages,

$$\bar{z}(t) = \frac{1}{\tau_\mathrm{D}}\int_0^t \mathrm{d}t'\ z(t')e^{-(t-t')/\tau_\mathrm{D}} \tag{12}$$

and

$$\sigma^2(t) = \frac{1}{\tau_\mathrm{D}}\int_0^t \mathrm{d}t'(z(t') - \bar{z}(t'))^2 e^{-(t-t')/\tau_\mathrm{D}} \tag{13}$$

The single parameter τ_D determines the time window used to estimate fluctuations in z. Equation 10 is no longer a valid estimator of the free energy when the Gaussians widths are adapted on-the-fly. A Torrie–Valleau-like correction developed for umbrella sampling[28] can be used to define an alternative free energy estimator,[29]

$$F_\Omega(z) = -\lim_{t\to\infty}[V(z, t) + k_\mathrm{B}T \ln \Omega(z, t) + \text{const.} \times \log t] \tag{14}$$

where $\Omega(z,t)$ is the accumulated histogram of the reaction coordinate z up to time t. The constant on the right-hand side is independent of z and t. The logarithmic divergence of eq 14 as $t \to \infty$ is irrelevant as long as the interest is free energy differences along z. A detailed presentation of the dynamically adapted version of well-tempered metadynamics is found in ref 29. In this work we computed free energy profiles both using eq 11 (which is technically not a valid free energy estimator when the adaptive Gaussians are used[29]) and eq 14, and they were found to be nearly identical using either of the two estimators.

Rigid Body Rotations. The adsorbed molecule was analyzed in terms of its orientation with respect to a reference configuration.[30] A simulation snapshot of TBP in water was chosen to be the reference configuration (time 0 in the simulation trajectory). The peptide is treated as a rigid body with an internal coordinate system that follows the molecule as it rotates in space, and which is measured with respect to the initial reference configuration. The rotation of the body is

DOI: 10.1021/acs.jpcc.5b02670
J. Phys. Chem. C 2015, 119, 18126–18139

described by the three angles formed by the corotating coordinate system and the initial coordinate system. These are the Euler angles (ϕ, θ, ψ), which are defined based on different conventions. The y-convention was used (rotation sequence: first ϕ around the z-axes, then θ around the y-axes, and finally ψ around the z-axes). The point defined by ϕ and θ coincides with the z-axes and points in the negative z-direction. The last rotation only matters when the surface is inhomogeneous. Each rotation step corresponds to one of the rotation matrices

$$\mathbf{R}_\phi = \begin{bmatrix} c & -s & 0 \\ s & c & 0 \\ 0 & 0 & 1 \end{bmatrix}, \quad \mathbf{R}_\theta = \begin{bmatrix} c & 0 & s \\ 0 & 1 & 0 \\ -s & 0 & c \end{bmatrix}, \quad \mathbf{R}_\psi = \begin{bmatrix} c & -s & 0 \\ s & c & 0 \\ 0 & 0 & 1 \end{bmatrix} \tag{15}$$

using the short-hand notations $c = \cos x$ and $s = \sin x$. The Euler angles were extracted from the total (3 × 3)-rotation matrix $\mathbf{R} = \mathbf{R}_\phi\, \mathbf{R}_\theta\, \mathbf{R}_\psi$.

The optimal rotation matrix $\mathbf{R}$ was obtained by solving the minimization problem of the root-mean-square-deviation (RMSD),

$$\min_{\mathbf{R},b} \sum_{i=1}^{n} \left\| \mathbf{R}\mathbf{p}_i - \mathbf{q}_i + \mathbf{b} \right\|^2, \quad \text{if} \quad \begin{cases} \mathbf{R} \in SO(3) \\ \mathbf{b} \in \mathbb{R}^3 \end{cases} \tag{16}$$

in a given simulation frame. The bars denote the matrix norm. $\mathbf{p}$ is the reference coordinate of the adsorbate and $\mathbf{q}$ is the coordinate of its present (instant) orientation. $\mathbf{R}$ and $\mathbf{b}$ are the optimal rotation and translation consistent with the transformation $\mathbf{p} \rightarrow \mathbf{q}$. The minimization is constrained by $\mathbf{R}$ being a SO(3) rotation matrix, i.e., orthogonal ($\mathbf{R}^T\mathbf{R} = 1$) and proper (det $\mathbf{R} = +1$). The translation vector $\mathbf{b}$ can be eliminated from the minimization problem by the use of centroid coordinates, $\mathbf{P}_i = \mathbf{p}_i - \bar{\mathbf{p}}$ and $\mathbf{Q}_i = \mathbf{q}_i - \bar{\mathbf{q}}$ (where $\bar{\mathbf{q}} = \sum_i \mathbf{q}/n$ and $\bar{\mathbf{p}} = \sum_i \mathbf{p}/n$ are the centers of geometry). Equation 16 now reads

$$\min_{\mathbf{R}} \{ \sum_{i=1}^{n} \mathrm{Tr}[(\mathbf{R}\mathbf{P}_i - \mathbf{Q}_i)^T (\mathbf{R}\mathbf{P}_i - \mathbf{Q}_i)] \} \tag{17}$$

where Tr (...) is the matrix trace, and the minimization is to be carried out under the conditions $\mathbf{R}\mathbf{R}^T = 1$ and det $\mathbf{R} = +1$. Equation 17 is a variant of a well-known matrix approximation problem (the "Procrustes Problem").[31] Defining a new matrix $\mathbf{B}^T = \sum_i^n \mathbf{P}_i\, \mathbf{Q}_i^T$ and its singular value decomposition $\mathbf{B} = \mathbf{U}\mathbf{S}\mathbf{V}^T$, the analytical solution to eq 17 is

$$\mathbf{R} = \mathbf{U} \begin{pmatrix} 1 & 0 & 0 \\ 0 & 1 & 0 \\ 0 & 0 & d \end{pmatrix} \mathbf{V}^T \tag{18}$$

with $d = \mathrm{sign}(\det(\mathbf{U}\mathbf{V}^T))$.

MATERIALS AND METHODS

Systems and Models. *TiO_2 Slabs.* Titanium surfaces in aqueous media are expected to be oxygen-covered under ambient conditions (neutral pH and biological salt concentration),[19−21] e.g., as implants[22] or nanoparticle surfaces. To mimic such conditions, we used a model with oxygen-terminated TiO_2 (100) surface slabs, consisting of layers of 2-coordinated oxygens on top of 5-coordinated titaniums (Ti−O−Ti bridges on the surface, the same setup as used in an accompanying TiO_2 force field parametrization by us[16] and similar to that of ref 32). We modeled the 2-coordinated oxygen surface without OH-termination, which corresponds to neutral pH for this surface.[16] Biological salt concentration (150 mM) corresponds to 1 salt molecule per 10 nm^3, which translates to at most 3 molecules for the small water volumes employed here, and will be neglected for the remainder of this paper.

The VESTA program[33] was used to replicate the TiO_2 rutile unit cell and terminate the supercells with (100) surfaces. Two TiO_2 slabs were created (Figure 1). The smaller corresponded

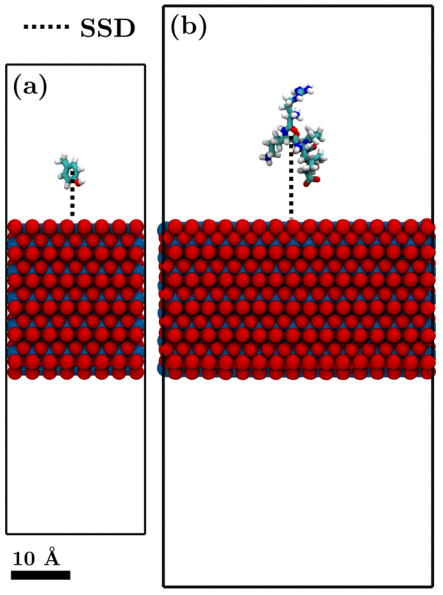

Figure 1. (a) Systems used to simulate adsorption of (a) side chain analogues (SCAs) and (b) titanium binding peptide (TBP) on TiO_2 (100). The surface separation distance (SSD) is the distance between the top layer in the TiO_2 slab and the center-of-mass of the molecule. Water is not shown for clarity.

to a 5 × 5 × 8 rutile supercell and was used to simulate adsorption of side chain analogues. The larger corresponded to a 5 × 8 × 16 rutile supercell and was used to simulate adsorption of a titanium binding peptide. The surface normals of the slabs were aligned with the z-direction of the simulation box (which was elongated with a vacuum in this direction). The slab thickness in both cases was h = 25 Å. The TiO_2 slabs were periodic in the x- and y-directions with a vacuum above and below. The final simulation box sizes were 23.6592 × 22.961 × 80 Å^3 (small slab) and 45.922 × 47.318 × 100 Å^3 (large slab). The force field recently developed by us[16] was used to describe TiO_2 interactions with water and solute molecules. The model uses a harmonic Ti−O bond and systematically optimized force field parameters based on the atomic coordination of TiO_2 and water adsorption enthalpy. This bonded TiO_2 model has been shown to reproduce the experimentally determined ζ-potential and heat of immersion of TiO_2/water interfaces, and the adsorbed structure of water on TiO_2 in agreement with density functional theory (DFT).[16] The force field parameters are summarized in Table 1. The TIP3P model[34] (in its original form with no hydrogen Lennard-Jones interactions) was used to model water, in agreement with the original parametrization.[16]

Side chain analogues (SCAs) are the molecules corresponding to truncating amino acid side chains at the protein backbone and replacing the C_α-carbon by a hydrogen. The

DOI: 10.1021/acs.jpcc.5b02670
J. Phys. Chem. C 2015, 119, 18126−18139

Table 1. Force Field Parameters for TiO_2 from Ref 16 Used in the Simulations

parameter	unit	value
σ_{Ti6}	Å	5.231
σ_{Ti5}	Å	4.6978
σ_{OT3}	Å	3.329
σ_{OT2}	Å	2.6951
ϵ_{Ti6}	kJ/mol	1.8168
ϵ_{Ti5}	kJ/mol	1.8151
ϵ_{O3}	kJ/mol	0.6480
ϵ_{O2}	kJ/mol	0.6226
q_{Ti6}	e	1.433
q_{Ti5}	e	1.8365
b_{Ti-O}	Å	1.9598
k_{Ti-O}	kJ/mol/Å^2	2113

present work covered 19 SCAs (Figure 2). They are the analogues of the 20 naturally occurring amino acids that are directly encoded for protein synthesis by the genetic code of eukaryotes, but excluding glycine and proline whose structures have no corresponding SCA. Histidine is found in two protonation states: δ-histidine (hydrogen on the δ-nitrogen) and ϵ-histidine (hydrogen on the ϵ-nitrogen). The net charges of the SCAs are −1 (negatively charged), 0 (neutral), or +1 (positively charged). The integer charge is enforced by giving the capping hydrogen the same partial charge as its hydrogen neighbors on the connecting (last) carbon atom, and then adjusting the partial charge on the last carbon atom accordingly. The 15 neutral SCAs (Figure 2 except the bottom row) have been used in previous computational studies.[35,36] Atomic coordinates and topologies for neutral SCAs were taken from ref 35. The charged SCAs (ARG, LYS, ASP, and GLU) were constructed by hand with PyMOL.[37] The AMBER force field[38] was used to model SCA interactions.

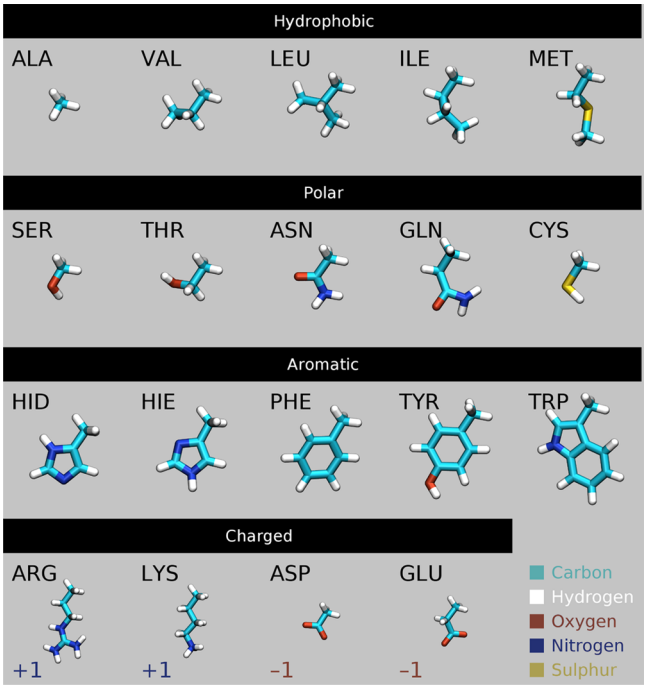

Figure 2. Side chain analogues (SCAs) to 18 (of 20) of the naturally occurring amino acids, classified as (i) hydrophobic without hydrogen bonding capability, (ii) polar with hydrogen bonding capability, (iii) aromatic with ring structures, and (iv) carrying net charge ±1. Histidine is considered in two forms: with protonation on the δ-nitrogen (HID) and the ϵ-nitrogen (HIE). SCAs corresponds to amino acid side chains that are truncated at the peptide backbone, and the C_α-carbon is replaced by a hydrogen.

The titanium binding peptide (TBP) is a peptide aptamer identified by phage display to interact electrostatically with Ti surfaces. The peptide sequence is ARG-LYS-LEU-PRO-ASP-ALA (RKLPDA), but there are to the best of the authors' knowledge no published atomic coordinates. PyMOL was therefore used to construct starting atomic coordinates for TBP. The AMBER force field[38] was used to model TBP interactions.

Nonbonded interaction parameters between TiO_2, SCA/TBP, and water were calculated by the Lorentz−Berthelot combination rules, as they are employed in the AMBER force field: $\sigma_{ij} = (\sigma_i + \sigma_j)/2$ and $\epsilon_{ij} = \sqrt{\epsilon_i \epsilon_j}$.

Simulation Protocols. *Unbiased Adsorption Simulations.* The simulations were carried out with Gromacs 4.6.5.[39,40] The adsorbates (SCAs or TBP) were placed above the TiO_2 slab. The systems were solvated with 950 (SCAs) or 4985 (TBP) water molecules and energy minimized for 1000 steps using a steepest gradient method. Equilibration was carried out for 100 ps in the NpT-ensemble (constant particle number, pressure, and temperature) using Berendsen weak coupling[41] thermostat and barostat. The temperature was kept at 300 K. The pressure tensor components were all set to 1 bar. Only the diagonal elements of the compressibility tensor κ were nonzero to keep a rectangular simulation box. The lateral directions (κ_{xx} and κ_{yy}) were set to 5×10^{-7} bar^{-1} (i.e., the inverse of the TiO_2 bulk modulus K_{TiO_2} = 200 GPa[42]) while the normal direction (κ_{zz}) was set to 5×10^{-5} bar^{-1}, corresponding to the inverse bulk modulus of water. The relaxation time constants of the thermostat and the barostat were set to 1.0 ps. Production simulations were performed under NVT conditions for 500 ns (at 300 K but with constant box volume). A Nose−Hoover thermostat[43,44] with relaxation time constant 5 ps was used to ensure correct ensemble fluctuations. Lennard-Jones interactions were truncated at 10 Å, and long-range electrostatics were treated with the Particle Mesh Ewald (PME) method[45,46] in all simulations.

Reaction Coordinates. Two reaction coordinates were used to describe adsorption in the simulated systems. The surface separation distance (SSD) measures how far the adsorbate is from the surface (Figure 1). The SSD was either calculated as the z-component of the distance between the centers-of-mass (COMs) of the surface atoms and the adsorbate (in the umbrella simulations or in the metadynamics simulations) according to

$$\mathrm{SSD} = \min_{i \in \mathrm{surface}} |\mathbf{R}_{\mathrm{mol}} - \mathbf{r}_i| \tag{19}$$

i.e., as the minimum distance between the COM of the adsorbate ($\mathbf{R}_{\mathrm{mol}}$) and the surface atoms ($\mathbf{r}_i$). The two definitions are equivalent. The minimum distance definition allows the adsorbate to cross the periodic z-boundary without artifacts since the slab is symmetric (the min-definition of the SSD can be used in other geometries as well). Since the metadynamics bias must be a continuous function (with continuous derivatives), the min-function is approximated with the analytical expression

DOI: 10.1021/acs.jpcc.5b02670
J. Phys. Chem. C 2015, 119, 18126−18139

$$\mathrm{SSD} = \frac{\beta}{\ln(\sum_{i\in\mathrm{surface}} e^{\beta/|\mathbf{R}_{\mathrm{mol}}-\mathbf{r}_i|})} \quad (20)$$

where β is a smoothing parameter with dimension of length. $i \in$ surface denotes all surface atoms in the TiO_2 slab. Equation 20 assigns large weights to small values of $\mathbf{R}_{\mathrm{mol}} - \mathbf{r}_i$ and becomes infinitely sharp (exact) in the limit $\beta \to \infty$. SSD as defined by eq 20 is in general very close to, but slightly smaller than, the actual minimum distance. β = 500 Å was used in all AWT-MetaD simulations.

A single reaction coordinate may not suffice to accurately sample adsorption of larger molecules to inorganic surfaces. The surface-bound molecule must overcome high free energy barriers to change from one adsorbed configuration to another. This sampling problem can be alleviated by a second reaction coordinate that accounts for the peptide's structure. A structural measure such as the root-mean-square-deviation (RMSD) from a reference configuration, or a geometric condition such as the peptide radius of gyration, are viable options for this reaction coordinate.[47] Another choice is the peptide's end-to-end distance (EED):

$$\mathrm{EED} = |\mathbf{R}_N - \mathbf{R}_C| \quad (21)$$

where $\mathbf{R}_N$ is the position of the C_α in the N-terminus (ARG) and $\mathbf{R}_C$ is the position of the C_α in the C-terminus (ALA). The EED is small when the peptide bends and larger when it unfolds. In order to reduce time spent by the adsorbate in the bulk region far from the surface, visiting of such states was prevented by setting a fictitious wall potential in addition to the metadynamics bias:

$$U_{\mathrm{wall}}(\mathrm{SSD}) = \kappa(\mathrm{SSD} - a)^4 \quad (22)$$

with the force constant being κ = 40 kJ mol^{-1} Å^{-4}, and the wall being positioned at a = 18 Å (SCAs) or a = 25 Å (TBP).

Biased Adsorption Simulations. SCA adsorption free energies as functions of the SSDs were calculated using umbrella sampling as implemented in Gromacs. The same systems and simulation conditions that were used in the unbiased simulations were used in the biased simulations. Starting configurations for each umbrella window were generated by placing the SCAs at the umbrella window centers (every 0.4 Å from the surface). Forty-one umbrella windows were used (0 ≤ SSD ≤ 16 Å), and the force constants were k = 10 kJ mol^{-1} Å^{-2}. Each window was subject to energy minimization, equilibration and finally production simulation for 50−100 ns (SER and THR required additional windows every 0.1 Å in the regime 0 ≤ SSD ≤ 5 Å to converge). Snapshots were saved every 5 ps. The total simulation time was 2−4 μs for each SCA. The weighted histogram analysis method (WHAM) as implemented in the `g_wham` analysis tool in Gromacs[39,40] was used to reconstruct the adsorption profiles.

Adaptive well-tempered metadynamics (AWT-MetaD) simulations were carried out with the PLUMED plug-in to Gromacs.[48] One-dimensional adsorption profiles as functions of the SSDs were calculated for the SCAs (same as the umbrella sampling simulations) and the two-dimensional free energy surface as a function of the SSD and the EED was calculated for TBP. The one-dimensional calculations were performed with a bias factor f = 10. Gaussians were added every 0.5 ps (the initial height was 1 kJ/mol). The Gaussian widths were updated according to eq 13, and the time window was computed using the parameter τ_D = 500 ps. The two-dimensional calculations used bias factor f = 20 and the initial height 2 kJ/mol and the rest of the parameters were kept the same. The production simulations for TBP adsorption lasted for 700 ns. One-dimensional free energy profiles for each CV were obtained from the two-dimensional free energy landscape using the projection formula

$$F_\omega(\omega) = k_B T \ln[\int e^{-F(\chi,\omega)/k_B T} d\chi] \quad (23)$$

where χ and ω was either the SSD or the EED.

RESULTS AND DISCUSSION

The Adsorption Profiles. Figure 3 shows the adsorption profiles of the strongest binding SCAs, SER and TYR, on TiO_2

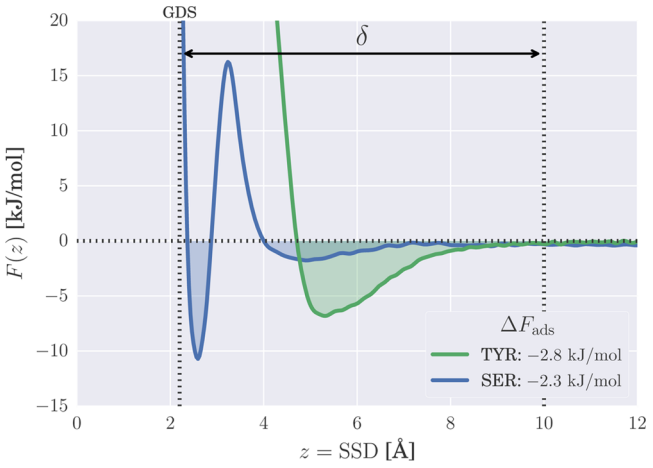

Figure 3. Adsorption free energy profiles for TYR and SER to TiO_2 (100) from adaptive well-tempered metadynamics simulations. z = SSD (surface separation distance) is the vertical distance from the top layer of the TiO_2 slab to the center-of-mass of the adsorbate. The bound region is defined by the adsorption layer thickness, δ = 8 Å, and extends from the Gibbs dividing surface (GDS) to where the profile flattens in the bulk. The shaded regions show the parts of the profiles that contribute to the adsorption free energy.

(100): the adsorption free energy $F(z)$ as a function of z = SSD. Three regimes can be identified. (1) Strong repulsion from atomic overlap close to the solid wall (small z). (2) An intermediate regime with minima next to the wall and/or between solvation layers (intermediate z). (3) Bulk regime far from the surface where the profile flattens, and the SCA is immersed in bulk waters. Depending on the size of the SCA and its ability to hydrogen bond, the SCAs can adsorb directly to the surface (SER) or outside the first solvation layer (TYR). The adsorption free energies were determined from these profiles by eq 6 with the adsorption layer thickness δ = 8 Å. Figure 4 shows the adsorption profiles for the SCAs obtained from umbrella sampling (US) simulations and adaptive well-tempered metadynamics (AWT-MetaD) simulations. The profiles were aligned to coincide at the surface (z = 0) and shifted vertically to be zero in the bulk. The adsorption free energies, being defined only up to an additive constant, are independent of these modifications. The two methods were found in good agreement and yields adsorption profiles with similar free energy minima, saddle points, and relative barrier heights.

Whether a metadynamics simulation is successful or not depends on choosing a proper reaction coordinate, which allows the system to move between states separated by high

DOI: 10.1021/acs.jpcc.5b02670
J. Phys. Chem. C 2015, 119, 18126−18139

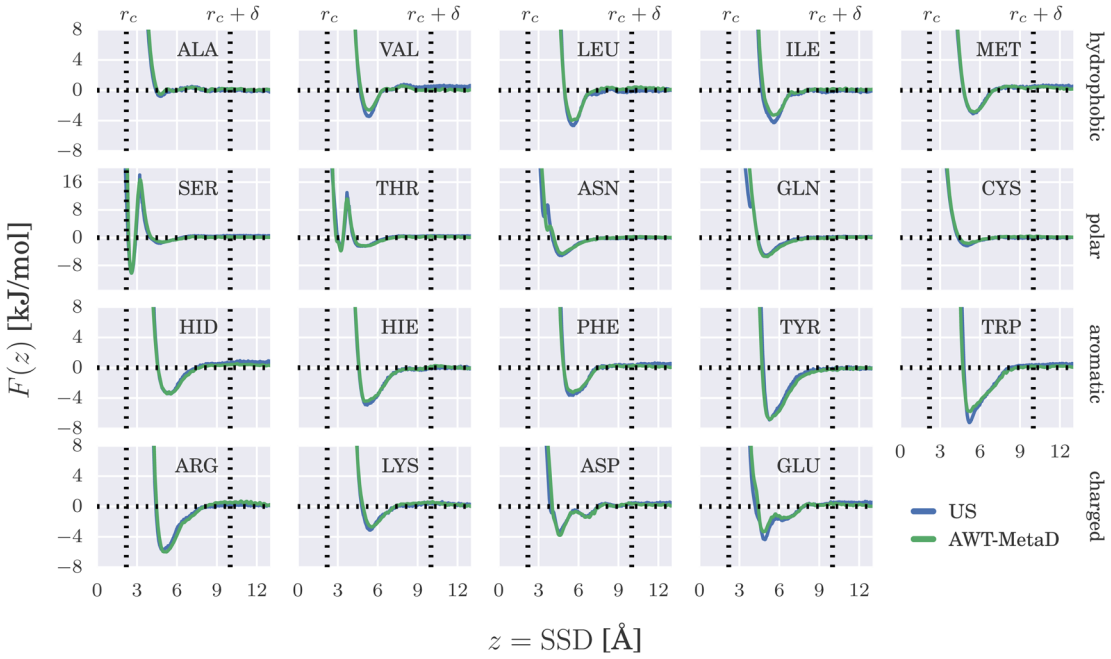

Figure 4. Adsorption free energy profiles as functions of the surface separation distance (SSD) for the SCAs. Each row corresponds to the classification of the SCAs in Figure 2. The profiles were obtained with umbrella sampling (US) simulations and adaptive well-tempered metadynamics (AWT-MetaD) simulations.

free energy barriers. Figure 5 shows the SSD during the AWT-MetaD simulation of the adsorption of SER on TiO_2 (100).

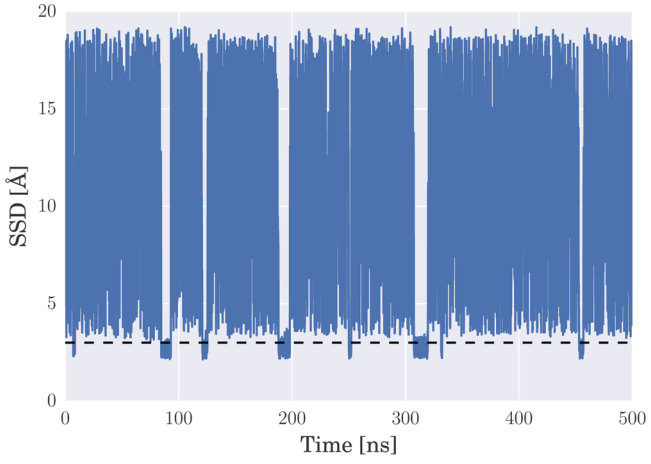

Figure 5. Surface separation distance (SSD) during AWT-MetaD simulation of SER adsorption on TiO_2 (100). The dashed line shows the position of the surface-bound water layer. SER has to "wait" for a water molecule to exchange with the bulk before binding directly to the TiO_2 surface. The associated free energy barrier is crossed 8 times during the 500 ns simulation.

SER is a polar molecule with hydrogen bond capability directly to the surface (Figure 2) through vacancies in the solvation layer. The occurrence of such a vacancy is a rare event, so SER may have to "wait" for a long time to be in a favorable position when the vacancy emerges. In the accelerated AWT-MetaD simulation, SER binds directly to the metal oxide surface through a vacancy in the solvation layer 8 times during the 500 ns simulation. Such sampling of a number of binding/unbinding events is outside the scope of unbiased simulations.

The US profiles are obtained from 41 independent simulation windows, each sampled for 100 ns, leaving the total sampling time for each SCA at 4 μs. The sampling was found satisfactory for all SCAs except those which penetrate the surface solvation layer (SER and THR), as discussed next. The profiles from AWT-MetaD simulations are well-converged within 500 ns, and requires a factor of 8 less sampling than the US simulations. The adsorption free energy is obtained by numerical integration of the adsorption profile according to eq 6. ΔF_{ads} is an exponential average of the adsorption profile and is therefore sensitive to its exact shape, in particular, to the width and depth of the energy minimum in the bound state. A slightly deeper minimum contributes exponentially to the integral in eq 6. The two SCAs that can adsorb directly to metal oxide surface by hydrogen bonding, SER and TYR, required extra sampling to get an accurate representation of the free energy barrier. They had to be simulated for 1.5 μs (AWT-MetaD) and with densely spaced umbrella windows (every 0.1 Å) in the region closest to the surface (US, 10 μs in total), respectively. The excessive sampling with umbrella simulations was needed to capture the narrow but high barrier due to the solvation layer.

The accuracy of calculated ΔF_{ads} based on the present profiles are ~0.5 kJ/mol for the US and for the MetaD simulations. This estimate was based on calculating ΔF_{ads} as a function of simulation time and monitoring the convergence. Better accuracy in US-profiles can be obtained by using more densely placed umbrella windows and/or a larger force constant. Better accuracy in AWT-MetaD-profiles can be obtained by decreasing the initial bias height and/or the deposition rate. The optimal strategy to calculate profiles depends on the usual trade-off between accuracy and speed, but the convergence of AWT-MetaD seem better than for US when calculating adsorption profiles, since the same level of accuracy can be reached within shorter simulation time.

DOI: 10.1021/acs.jpcc.5b02670
J. Phys. Chem. C 2015, 119, 18126−18139

SCA Adsorption on TiO_2 (100). The SCAs can be classified into four groups (Figure 2): Hydrophobic, polar, aromatic and charged. Hydrophobic SCAs consist of 1−4 linked or branched hydrocarbon chains (and MET incorporates a sulfur atom in the hydrocarbon chain). Polar SCAs are terminated with hydrogens connected to atoms with strong (O), moderate (N) or weak (S) electronegativity and can form hydrogen bonds with varying strengths. Aromatic SCAs consist of a five- and/or six-membered aromatic ring that is decorated with terminating N- or O-groups. Charged SCAs are hydrocarbon chains terminated with either amine (positively charged) or hydroxyl groups (negatively charged). Their net charges are ±1.

Table 2 and Figure 6 shows the SCA adsorption free energies calculated by numerical integration of the adsorption profiles according to eq 6. Table 2 is sorted by descending binding strength (based on US simulations) and is divided into three parts: binding, weakly binding, and nonbinding.

Table 2. Adsorption Free Energies (in kJ/mol) for Side Chain Analogues (SCA) on the (100) Surface of Rutile TiO_2 from Umbrella Sampling (US) and Adaptive Well-Tempered Metadynamics (AWT-MetaD) simulations[a]

SCA	%[b]	class[c]	T-group[d]	N[e]	US	AWT-MD
SER	7.4	P	OH	6	−2.56	−2.34
TYR	3.3	A	OH	16	−2.45	−2.82
TRP	1.3	A	NH	19	−2.44	−1.99
ARG	5.2	C^+	NH_2	19	−1.85	−2.05
ASN	4.6	P	NH_2	9	−1.45	−1.15
HIE	2.2	A	NH	12	−1.38	−1.20
GLN	4.1	P	NH_2	12	−1.28	−1.67
GLU	6.3	C^-	O	10	−0.73	−0.29
ILE	5.5	H	CH_3	14	−0.70	−0.21
LEU	9.1	H	CH_3	14	−0.64	−0.28
PHE	3.9	A	CH	15	−0.44	−0.27
ASP	5.2	C^-	O	7	−0.37	−0.47
HID	2.2	A	NH	12	−0.35	−0.47
THR	6.0	P	OH	9	−0.34	−0.51
MET	2.8	H	CH_3	12	0.03	0.06
LYS	5.8	C^+	NH_2	17	0.05	0.23
CYS	1.8	P	SH	6	0.11	0.43
VAL	6.5	H	CH_3	11	0.13	0.36
ALA	7.5	H	CH_3	5	0.71	0.83

[a]SCAs are sorted in order of (US) binding strength. The horizontal lines delimit binding (top), weakly binding (middle) and non-binding (bottom) SCAs. When $F_{ads} \geq 0$, the SCA does not adsorb on the surface. [b]Frequency of occurrence of each amino acid in proteins (from ref 49). [c]H = hydrophobic, *P* = polar, A = aromatic, and C = charged. [d]Terminating group in SCA. [e]Total number of atoms in SCA.

The strongest binding SCAs are found to be the polar and the aromatic ones, while hydrophobic SCAs have lower affinities for the surface. There is no consistent binding trend for the charged SCAs; in other words: the dipole−charge interaction emerging from the Ti and O surface layers with the charged SCAs is not strong enough to determine the adsorption behavior. The reason is that electrostatic interactions are shielded at the surface by tightly bound waters. The salt concentration in biological environments is usually ∼150 mM, and could potentially impact the behavior of protein adsorption on TiO_2 by changing the structure of the solvation layer. The negatively charged SCAs (ASP and GLU) are attracted to the solvation layer as hydrogen bond acceptors, but the effect is weak. The positively charged SCAs (ARG and LYS) also primarily serve as donors, and hydrogen bonding therefore plays a minor effect for these SCAs. The difference in adsorption free energy between ARG and LYS is 2 kJ/mol, which is significantly larger than the sampling error sampling (0.5 kJ/mol). The preferred binding orientation of both are flat on the surface, and the additional NH_2-groups in ARG can hydrogen bond to the solvation layer.

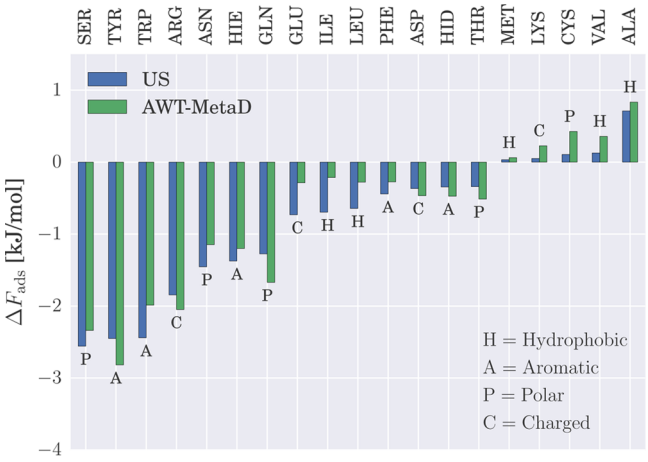

Figure 6. Adsorption free energies for the 19 investigated SCAs. ΔF_{ads} was obtained by the use of eq 6 to numerically integrate the adsorption profiles from this figure. Units in kJ/mol. .

The binding SCAs have O- or N-containing terminating groups that form hydrogen bonds to the tightly bound surface waters. SER is the strongest binder because it can penetrate the solvation layer and hydrogen bond as a donor directly to the metal oxide surface. SER adsorbs by fitting into a vacant binding site which emerge when surface waters exchange with bulk waters. To replace a surface water, the SER molecule needs to cross a free energy barrier of 15 kJ/mol (Figure 3) to find a deep but narrow minimum (10 kJ/mol, 1 Å) closest to the surface. A similar barrier was also found in adsorption simulations of methanol (analogue to serine) on rutile (110).[17]

In contrast, THR can also use its OH-group to form a hydrogen bond directly to the surface, but does not fit into a single (vacant) water binding site because of its larger size. The probability of two adjacent water binding sites being vacant is low, and therefore the barrier remains, but the value of the free energy in the first minimum is close to zero (Figure 4).

The position of a terminating OH- or NH-group and its ability to hydrogen bond can make a difference in whether a SCA will adsorb on the surface or not. Specifically, the difference between HID and HIE (both aromatic SCAs but with a proton on either the δ- or ϵ-nitrogen) and between TYR or TRP and PHE (all aromatic, but PHE lacks hydrogen bonding capability). The difference between HID and HIE is 1 kJ/mol. The difference between TYR/TRP and PHE is 1.5 kJ/mol. In the latter case, the hydrogen bonding to the surface solvation layer is crucial for adsorption to take place. Whether the bulky double ring structure of TRP is an advantage or a drawback for adsorption could not be settled from the adsorption profiles or the adsorption free energy. These two subtle effects are reproduced by both the US and the AWT-MetaD simulations.

The interactions between nitrogen atoms or oxygen atoms and the surface are in general favorable, while carbon (and

DOI: 10.1021/acs.jpcc.5b02670
J. Phys. Chem. C 2015, 119, 18126−18139

sulfur) are unfavorable, as expected for a hydrophilic surface. The simulation data shows no relation between the binding strength and the size of the SCA (Table 2). The free energy per atom, $\Delta F/N$, is similar to ΔF itself (data not shown). The adsorption free energies for the binding group in Table 2 are 0.5−1.5 k_BT, which is significantly weaker than the binding of SCAs to gold surfaces[13] but similar to the SCA adsorption free energies reported for the metal oxide ZnO.[50]

One important result from the present work is that different functional groups (amine-, hydroxyl-, and methyl groups) have different binding affinities for the TiO_2 (100) surface. The SCAs with the largest affinities, namely, polar and aromatic SCAs, can be expected to be commonly occurring in peptides and proteins that bind to TiO_2 surfaces. Amine groups were found to bind to TiO_2 in both polar, aromatic and charged SCAs.

Simulations of selected side chain analogues on the TiO_2 (110) surface[17] showed generally stronger affinities for the surface, but depended strongly on the specific surface structure, i.e., whether the adsorbate fitted between two "rails" of bridging oxygens to gain access to exposed Ti atoms in the basal plane of the surface. On the unstructured (100) surface employed in this work (which is chosen to be representative for titanium surfaces in biological environments), the only direct contact possible for adsorbates is by competing with surface-bound waters through hydrogen bonding to surface oxygens (as seen for SER and THR). The outcome is weaker binding through the intermediate surface waters. We note that hydrophobic side chains did not bind to TiO_2 in either study.

The protonation degree is expected to be low (1%) at neutral surface pH (which is the target of the present modeling). However, if the binding strengths of protonated surface sites are substantially (orders of magnitude) larger than disassociated ones, a small fraction of protonated sites could have a large impact on binding trends. This effect can be neglected when binding strengths between protonated/deprotonated surface sites are similar in order of magnitude.

Overall, binding of individual SCAs to the TiO_2 (100) surface can be considered as weak with binding free energies of a few kJ/mol. Nevertheless, the accumulated effect of many SCAs in a protein can be considerable. One can speculate that proteins with high fractions of the side chains from the top of Table 2 would have higher binding affinity to TiO_2 surfaces, and that a protein would prefer to bind to the surface by the side with higher content of those SCAs. Such information is important, for example, to predict the composition and surface properties of the protein corona of nanoparticles in biological fluids, which is relevant to the understanding of nanotoxicity for TiO_2.

TBP Adsorption on TiO_2 (100). We carried out both unbiased and enhanced sampling simulations of TBP near the TiO_2 (100) surface, with the aim to investigate collective effects of amino acids on peptide adsorption. Figure 7 shows representative snapshots during an *unbiased* simulation of TBP adsorption on TiO_2 (100). Figure 8 shows (a) the surface separation distance (SSD), (b) the peptide end-to-end distance (EED) and (c) the peptide root-mean-square-deviation (RMSD) during the same simulation. (The definitions of the SSD, the EED, and the RMSD are given in eq 20, eq 21, and eq 16, respectively.) Figure 9 shows the adsorbed configurations of the binding modes in atomistic detail.

TBP adsorbs on the TiO_2 surface within 10 ns of simulation time, and stays bound for more than 300 ns. During this time,

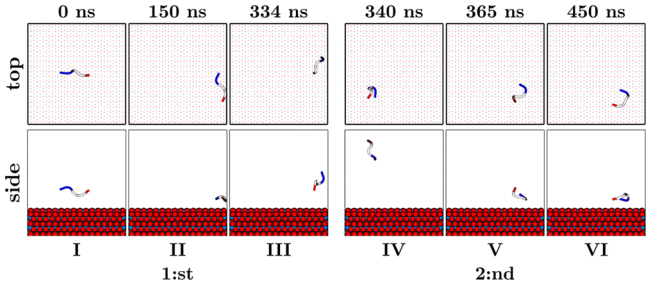

Figure 7. Representative snapshots from the unbiased simulation of TBP on the TiO_2 (100) surface. The peptide quickly adsorbs on the surface and stays bound in the same configuration (1:st binding mode, snapshots I−III) for 334 ns. The peptide structure changes during release, and it readsorbs in a more compact configuration (2:nd binding mode, snapshots IV−VI). TBP stays bound with this structure for the remainder of the simulation time.

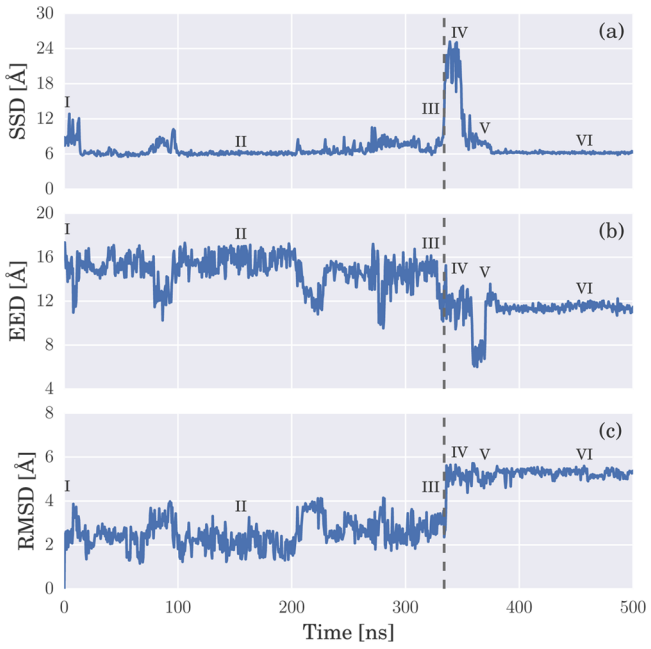

Figure 8. Unbiased simulation of TBP on the TiO_2 (100) surface while monitoring (a) the surface separation distance (SSD), (b) the end-to-end distance (EED), and (c) the root-mean-square deviation (RMSD) of TBP. The Roman numerals correspond to the snapshots from the simulation trajectory shown in Figure 7.

TBP does not interact directly with the surface but is adsorbed through surface-bound waters (the first solvation layer). When TBP is released from the surface after 334 ns of simulation time, its structure changes as it comes off the surface and the peptide rebinds with a new shape after diffusing in the bulk water for 20 ns. There is still a water layer present between the peptide and the surface. The TBP structure during the first binding time (up to 334 ns, snapshots I−III in Figure 7) will be called the "1:st binding mode". The TBP structure during the second time of binding (snapshots IV−VI in Figure 7) will be referred to as the "2:nd binding mode".

The first binding mode is worm-like and similar to the peptide's preferred configuration in the bulk solvent; TBP is flexible and diffuses more or less freely on the surface (see snapshots I−III in Figure 7 and Figure 9a,d). In the second binding mode, the charged residues at the peptide N-terminus (ARG) and C-terminus (ASP) form a salt bridge, which locks

DOI: 10.1021/acs.jpcc.5b02670
J. Phys. Chem. C 2015, 119, 18126−18139

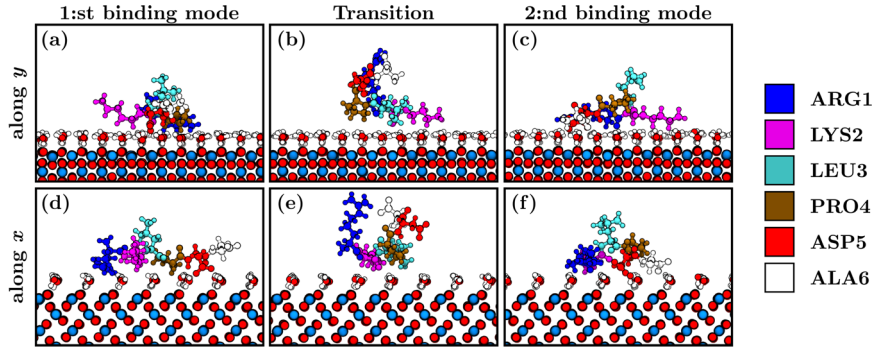

Figure 9. Ball-and-stick representations of adsorbed configurations and the first water layer during the unbiased simulation, along the *y*-axis (a−c) and along the *x*-axis (d−f). Panels a and d correspond to the 1:st binding mode (snapshot II from Figures 7 and 8), panels b and e correspond to the transition after rebinding (snapshot V), and panels c and f corresponds to the 2:nd binding mode (snapshot VI). Each amino acid is color coded in accordance with the panel to the right.

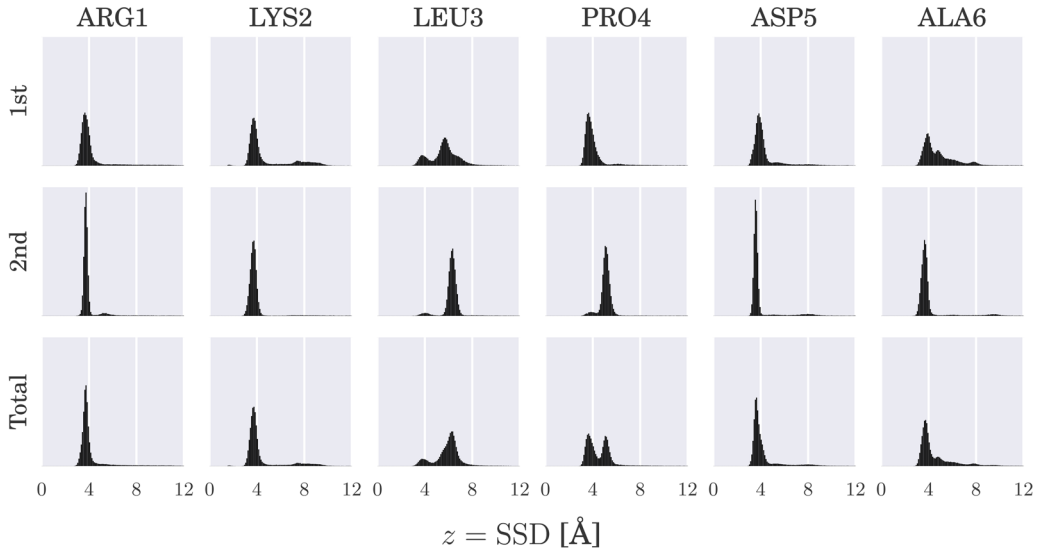

Figure 10. Residue-based SSD histograms for the residues in the TBP sequence during the unbiased simulation. The top row shows the 1:st binding mode, the middle row shows the 2:nd binding mode, and the bottom row shows the entire trajectory. The LEU3 and PRO4 histograms are bimodal for the total trajectory, which implies two distinct positions for the two binding modes.

the peptide in a compact, "C"-shaped, structure that is strongly adsorbed on the surface (Figure 9f). A similar shape was determined in NMR experiments for TBP adsorbed on titania nanoparticles.[10] The peptide structure is intact in both binding modes, but the magnitude of the SSD fluctuations are larger for the 1:st binding mode as compared to the 2:nd. The EED varies between 16 Å (1:st mode) to 12 Å (2:nd mode) but the fluctuations in the 2:nd mode is practically zero which shows that this is a strongly bound state. We note that the adsorption mechanism observed in this single unbiased simulation does not exclude the possibility of other binding pathways.

The binding modes from the unbiased simulation were further analyzed in terms of position and orientation. Figure 10 shows position histograms for the binding modes, where each column corresponds to a residue in the TBP sequence. The top row is calculated for the first binding event (up to 334 ns), the middle row is calculated for the second binding event (from 334 ns), and the bottom row is the distribution from the complete trajectory (1:st and 2:nd). The histograms are based on the SSD of the individual TBP residues and are normalized as probability distributions. The distributions for the 1:st mode are unimodal for charged residues (ARG1, LYS2, and ASP5) or smeared out (LEU3 and ALA6). The distributions for the 2:nd mode are narrower than the 1:st mode. In particular, the charged residues near the termini (ARG1 and ASP5) have very specific positions, because the 2:nd mode is a more folded peptide structure. The salt bridge formed by the opposite charges in ARG1 and ASP5 stabilizes the peptide structure and leads to small EED- and SSD-fluctuations. The neutral side chains LEU3 and PRO4 constitute the "bend" in the C-shape and reside around 6 Å, compared to 4 Å in the 1:st mode, from the surface. The total distributions (1:st and 2:nd binding mode) of PRO4 and (partially) LEU3 are bimodal, with one peak from the 1:st mode and one peak from the 2:nd mode. In all cases, TBP residues bind to the first surface solvation layer and not directly to the metal oxide surface (Figure 9).

The adsorbed peptide structure was also analyzed in terms of its orientation. The analysis was performed by calculating the optimal rotation matrix **R** (eq 18) for the peptide with respect to its starting structure in the bulk at all simulation times. The Euler angles were extracted from **R**, and probability distributions were calculated based on the first (1:st binding mode) part of the simulation trajectory, the second (2:nd binding mode) part of the simulation trajectory, and the total simulation trajectory. Figure 11 shows the angle distributions. The distributions for the angles θ and ψ are unimodal (have

DOI: 10.1021/acs.jpcc.5b02670
J. Phys. Chem. C 2015, 119, 18126−18139

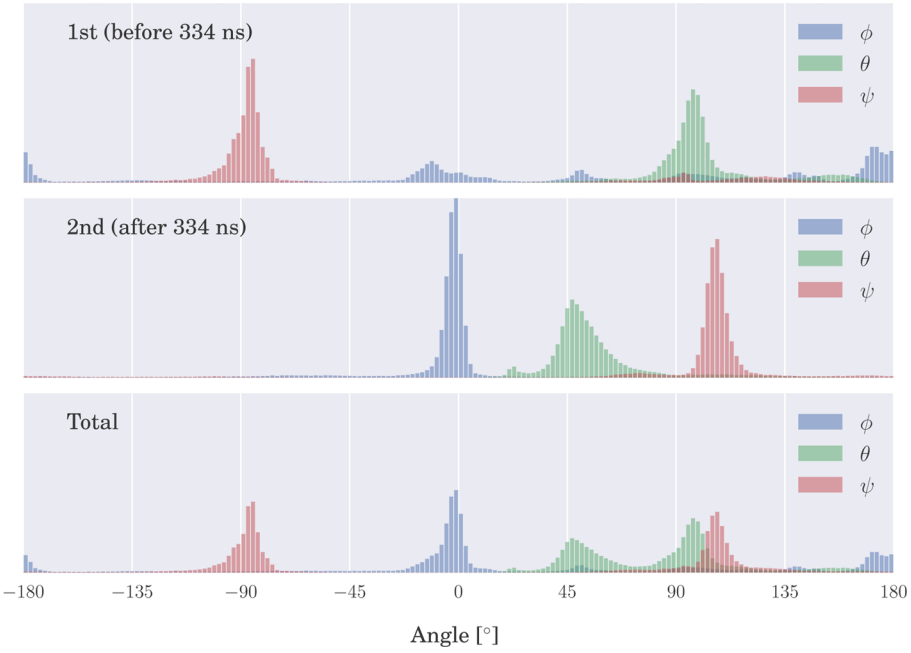

Figure 11. Normalized histograms for the Euler angles from the unbiased TBP simulation. The top panel shows the 1:st binding mode (before 334 ns), the middle panel shows the 2:nd binding mode (after 334 ns), and the bottom panel shows the entire trajectory.

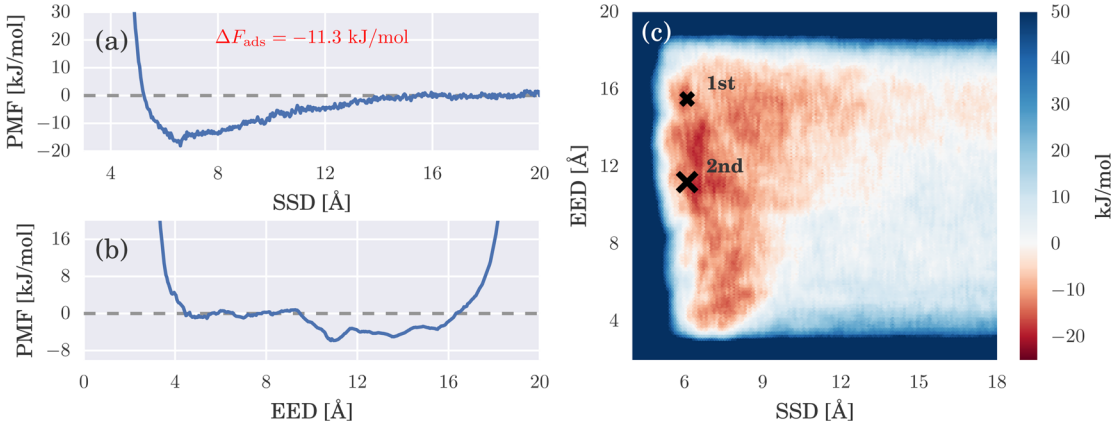

Figure 12. AWT-MetaD simulation of adsorption of TBP on the TiO_2 (100) surface. (a) Adsorption profile (potential of mean force, PMF) as a function of the SSD. The adsorption layer thickness is δ = 10 Å and the adsorption free energy is ΔF_{ads} = −11.3 kJ/mol. (b) Potential of mean force as a function of the EED. The region EED > 10 Å is preferred by 5 kJ/mol to the region EED < 10 Å. (c) The two-dimensional free energy landscape; the two binding modes identified from the unbiased simulation are marked with crosses.

one peak) for each binding mode with maxima at 98° and −86°, respectively, but the distribution of ϕ is multimodal for the 1:st binding mode, with the most pronounced maximum at 175°. The ϕ-distribution for the 2:nd binding mode is unimodal like the other angles. The preferred values are ϕ = 0°, θ = 48° and ψ = 107°. The total angular distributions are bimodal, where the maxima corresponds to preferred orientations of the corresponding binding mode. The cumulative picture of TBP adsorption on TiO_2 (100) is that the worm-like peptide is firmly adsorbed on the surface in the 1:st binding mode but can rotate freely by "wiggling" on the surface. In the 2:nd binding mode, the folded structure is stabilized by the formation of a salt bridge between ARG1 and ASP5, which locks the peptide in place. In both binding modes (worm-like and folded), the peptide adsorbs parallel (not upright) to the surface.

Adsorption statistics (binding/unbinding) for TBP can not be calculated from a single event. Therefore, metadynamics simulations were performed for TBP using the surface separation distance (SSD) and the peptide end-to-end distance (EED) as two simultaneous reaction coordinates. Figure 12 shows the two-dimensional free energy landscape obtained from AWT-MetaD simulations of TBP adsorption on the TiO_2 (100) surface. Panels a and b show the free energy projected along the SSD and the EED, respectively. Panel c shows the two-dimensional free energy landscape as a function of both reaction coordinates at the same time. The binding modes identified from the unbiased simulations are marked with crosses in Figure 12. The adsorption free energy of TBP on TiO_2 (100) was calculated to be ΔF_{ads} = −11.3 ± 2 kJ/mol (error estimate determined by monitoring convergence of ΔF_{ads} as a function of simulation time), corresponding to an equilibrium constant $K \sim 10^{-2}$. The adsorption profile contains

DOI: 10.1021/acs.jpcc.5b02670
J. Phys. Chem. C 2015, 119, 18126−18139

no barrier but a free energy minimum of depth 15 kJ/mol when TBP is near the surface. The presence of the surface is felt until the COM of the peptide is further than 16 Å away, and there is always a solvation layer present between the surface and the peptide, even when the peptide is adsorbed.

The free energy depends weakly on the end-to-end (EED) distance. Peptide structures with EED < 10 Å are unfavored by 5 kJ/mol (2 k_BT) compared to structures with 1 < EED < 16 Å, but the calculations can not separate the 1:st and the 2:nd binding mode based on the EED (the 1:st binding mode is characterized by EED ≈ 12 Å, and the 2:nd binding mode is characterized by EED ≈ 16 Å). The weak dependence of the free energy on the EED suggests that it may be possible to find alternative reaction coordinates to change the peptide structure of the adsorbed state. Geometric conditions such as the radius of gyration, are similar to the EED and can not be excepted to perform better. One approach with potential is to reduce the barrier of desolvation of the interface,[51] i.e., to force surface waters to release when the peptide is at the interface.

The total binding energy of TBP to the TiO_2 surface, −11.3 kJ/mol, is significantly lower than the sum of individual SCA contributions (proline was not included in the SCA adsorption free energy calculations, but its contribution is expected to be weak because it fluctuates between the first and second hydration layers in the bound state). In other words, TBP is worthy of its name and binds stronger to TiO_2 than is expected from the individual fragments in its sequence. The enhanced binding for this particular peptide sequence is the collective effects of its specific hydration structure, as suggested in earlier simulations focused on finding the rationale behind the Ti/Si-selection mechanism for TBP on oxidized titanium and silicon surfaces.[23] The present simulations expand on previous efforts to model TBP interacting with titania surfaces,[18] by employing advanced sampling techniques to overcome earlier limitations in probing the entropic contribution to TBP adsorption. In particular, the formation of a salt bridge between ARG1 and ASP5 in the compact second binding mode, previously unidentified, was found to act as the main stabilizing factor. This binding structure is also found in NMR experiments.[10]

Finally, we note that biomolecular binding trends and peptide adsorption behavior can be influenced by major changes in outer conditions such as pH shifts, high ionic strengths, and/or differering planes/crystal phases of the inorganic material.[52] For silica surfaces, for instance, the recognition to similar peptide sequences has been reported to be low as the surface termination is changed.[53,54] An interesting avenue for future simulation work on biomolecular adsorption on titania surfaces would be systematic studies of changing pH and/or degree of ionization for the surface.

CONCLUSIONS

Adsorption profiles were determined for 19 amino acid side chain analogues on the TiO_2 (100) surface using microsecond simulations with enhanced sampling. Good agreement were found for profiles determined using umbrella sampling simulations and the adaptive well-tempered metadynamics (AWT-MetaD) method. AWT-MetaD calculations were found more efficient compared to the US simulations as the former required substantially less sampling to obtain convergence. Adsorption free energies were calculated from the profiles and analyzed based on the chemical properties of the SCAs. Two polar SCAs, SER and THR, were found to be able to penetrate the tightly bound waters at the surface and bind to TiO_2 directly, while other SCAs adsorbed to the first solvation layer. The energy barrier for the molecule to penetrate the solvation layer was found to be ∼10 k_BT. Polar and aromatic side chains were found to bind to TiO_2 (100) with binding free energies of a few kJ/mol, while hydrophobic SCA showed weak or no binding. Data on SCAs binding energies can be used for qualitative estimation of binding affinities and binding modes of proteins to TiO_2 surfaces. Furthermore, calculated SCA adsorption profiles can be used as potentials of mean force to parametrize coarse-grained models for TiO_2 surface−biomolecule interactions.

Two binding modes were identified for a titanium binding peptide (TBP) on the TiO_2 surface; both represent structures where the peptide binds flat on the surface. The 1:st binding mode was an extended structure where the peptide could rotate on the surface. The 2:nd binding mode was a compact structure, stabilized by the salt bridge formation between ARG1 and ASP5 in the peptide sequence. A similar "C-shaped" structure has been identified as the binding structure in NMR experiments.[10] A molecular picture of the mechanism of TBP adsorption on TiO_2 was given in terms of two-dimensional free energy landscapes. The adsorption free energy was calculated from the adsorption profile to be −11.3 kJ/mol, and adsorption was found to be enhanced compared to individual amino acid contributions, due to the specific arrangement of the peptide at the hydrated surface.

In summary, the simulations emphasized the role of the solvation layer in biomolecular adsorption at inorganic surfaces. Future work will investigate adsorption on other materials, and develop improved methods for efficient sampling of biomolecules at inorganic interfaces.

AUTHOR INFORMATION

Corresponding Author

*Phone: +46-8-161193; E-mail: alexander.lyubartsev@mmk.su.se.

Notes

The authors declare no competing financial interest.

ACKNOWLEDGMENTS

This work was supported by the European 7-th Framework program (MembraneNanoPart project) and by the Swedish Research Council (Grant No. 621-2013-4260). The simulations were performed on resources provided by the Swedish National Infrastructure for Computing.

REFERENCES

(1) Kasemo, B. Biological Surface Science. *Curr. Opin. Solid State Mater. Sci.* **1998**, *3*, 451−459.
(2) Silva-Bermudez, P.; Rodil, S. E. An Overview of Protein Adsorption on Metal Oxide Coatings For Biomedical Implants. *Surf. Coat. Technol.* **2013**, *233*, 147−158.
(3) Nel, A.; Xia, T.; Mädler, L.; Li, N. Toxic Potential of Materials at the Nanolevel. *Science* **2006**, *311*, 622−627.
(4) Dimilla, P. A.; Albelda, S. M.; Quinn, J. A. Adsorption and Elution of Extracellular Matrix Proteins On Non-Tissue Culture Polystyrene Petri Dishes. *J. Colloid Interface Sci.* **1992**, *153*, 212−225.
(5) Yang, Y.; Cavin, R.; Ong, J. L. Protein Adsorption on Titanium Surfaces and Their Effect On Osteoblast Attachment. *J. Biomed. Mater. Res.* **2003**, *67A*, 344−349.
(6) Weir, A.; Westerhoff, P.; Fabricius, L.; Hristovski, K.; von Goetz, N. Titanium Dioxide Nanoparticles in Food and Personal Care Products. *Environ. Sci. Technol.* **2012**, *46*, 2242−2250.

DOI: 10.1021/acs.jpcc.5b02670
J. Phys. Chem. C 2015, 119, 18126−18139

(7) Teow, Y.; Asharani, P. V.; Hande, M. P.; Valiyaveettil, S. Health Impact and Safety of Engineered Nanomaterials. *Chem. Commun.* **2011**, *47*, 7025−7038.
(8) Sano, K.-I.; Shiba, K. A Hexapeptide Motif that Electrostatically Binds to the Surface of Titanium. *J. Am. Chem. Soc.* **2003**, *125*, 14234−14235.
(9) Sano, K.-I.; Sasaki, H.; Shiba, K. Specificity and Biomineralization Activities of Ti-Binding Peptide-1 (TBP-1). *Langmuir* **2005**, *21*, 3090−3095.
(10) Mirau, P. A.; Naik, R. R.; Gehring, P. Structure of Peptides on Metal Oxide Surfaces Probed by NMR. *J. Am. Chem. Soc.* **2011**, *133*, 18243−18248.
(11) Latour, R. A. Molecular Simulation of Protein-Surface Interactions: Benefits, Problems, Solutions, and Future Directions (Review). *Biointerphases* **2008**, *3*, FC2−FC12.
(12) Deighan, M.; Pfaendtner, J. Exhaustively Sampling Peptide Adsorption with Metadynamics. *Langmuir* **2013**, *29*, 7999−8009.
(13) Hoefling, M.; Iori, F.; Corni, S.; Gottschalk, K.-E. Interaction of Amino Acids with the Au(111) Surface: Adsorption Free Energies from Molecular Dynamics Simulations. *Langmuir* **2010**, *26*, 8347−8351.
(14) Mücksch, C.; Urbassek, H. M. Enhancing Protein Adsorption Simulations by Using Accelerated Molecular Dynamics. *PLoS One* **2013**, *8*, e64883.
(15) Heinz, H.; Lin, T.-J.; Kishore Mishra, R.; Emami, F. S. Thermodynamically Consistent Force Fields for the Assembly of Inorganic, Organic, and Biological Nanostructures: The INTERFACE Force Field. *Langmuir* **2013**, *29*, 1754−1765.
(16) Brandt, E. G.; Lyubartsev, A. J. *J. Phys. Chem. C* **2015**, DOI: 10.1021/acs.jpcc.5b02669.
(17) Monti, S.; Walsh, T. R. Free Energy Calculations of the Adsorption of Amino Acid Analogues at the Aqueous Titania Interface. *J. Phys. Chem. C* **2010**, *114*, 22197−22206.
(18) Skelton, A. A.; Liang, T.; Walsh, T. R. Interplay of Sequence, Conformation, and Binding at the Peptide-Titania Interface as Mediated by Water. *ACS Appl. Mater. Interfaces* **2009**, *1*, 1482−1491.
(19) Healy, K. E.; Ducheyne, P. Hydration and Preferential Molecular Adsorption on Titanium in Vitro. *Biomaterials* **1992**, *13*, 553−561.
(20) Lausmaa, J.; Kasemo, B.; Mattsson, H. Surface Spectroscopic Characterization of Titanium Implant Materials. *Appl. Surf. Sci.* **1990**, *44*, 133−146.
(21) Roddick-Lanzilotta, A. D.; Connor, P. A.; McQuillan, A. J. An In Situ Infrared Spectroscopic Study of the Adsorption of Lysine to TiO_2 from an Aqueous Solution. *Langmuir* **1998**, *14*, 6479−6484.
(22) Jones, F. H. Teeth and Bones: Applications of Surface Science to Dental Materials and Related Biomaterials. *Surf. Sci. Rep.* **2001**, *42*, 75−205.
(23) Schneider, J.; Colombi Ciacchi, L. Specific Material Recognition by Small Peptides Mediated by the Interfacial Solvent Structure. *J. Am. Chem. Soc.* **2012**, *134*, 2407−2413.
(24) Wei, Y.; Latour, R. A. Determination of the Adsorption Free Energy for Peptide-Surface Interactions by SPR Spectroscopy. *Langmuir* **2008**, *24*, 6721−6729.
(25) Kumar, S.; Rosenberg, J. M.; Bouzida, D.; Swendsen, R. H.; Kollman, P. A. THE Weighted Histogram Analysis Method for Free-Energy Calculations on Biomolecules. I. The Method. *J. Comput. Chem.* **1992**, *13*, 1011−1021.
(26) Laio, A.; Parrinello, M. Escaping Free-Energy Minima. *Proc. Natl. Acad. Sci. U. S. A.* **2002**, *99*, 12562−12566.
(27) Barducci, A.; Bussi, G.; Parrinello, M. Well-Tempered Metadynamics: A Smoothly Converging and Tunable Free-Energy Method. *Phys. Rev. Lett.* **2008**, *100*, 020603.
(28) Torrie, G. M.; Valleau, J. P. Nonphysical Sampling Distributions in Monte Carlo Free-Energy Estimation: Umbrella Sampling. *J. Comput. Phys.* **1977**, *23*, 187−199.
(29) Branduardi, D.; Bussi, G.; Parrinello, M. Metadynamics with Adaptive Gaussians. *J. Chem. Theory Comput.* **2012**, *8*, 2247−2254.
(30) Sun, Y.; Welsh, W. J.; Latour, R. A. Prediction of the Orientations of Adsorbed Protein Using an Empirical Energy Function with Implicit Solvation. *Langmuir* **2005**, *21*, 5616−5626.
(31) Gower, J. C., Dijksterhuis, G. B. *Procrustes Problems*; Oxford University Press: Oxford, U.K., 2004.
(32) Köppen, S.; Langel, W. Simulation of the Interface of (100) Rutile with Aqueous Ionic Solution. *Surf. Sci.* **2006**, *600*, 2040−2050.
(33) Momma, K.; Izumi, F. *VESTA3* for Three-Dimensional Visualization of Crystal, Volumetric and Morphology Data. *J. Appl. Crystallogr.* **2011**, *44*, 1272−1276.
(34) Jorgensen, W. L.; Chandrasekhar, J.; Madura, J. D.; Impey, R. W.; Klein, M. L. Comparison of Simple Potential Functions For Simulating Liquid Water. *J. Chem. Phys.* **1983**, *79*, 926−935.
(35) Shirts, R. M.; Pitera, J. W.; Swope, W. C.; Pande, V. S. Extremely Precise Free Energy Calculations of Amino Acid Side Chain Analogs: Comparison of Common Molecular Mechanics Force Fields for Proteins. *J. Chem. Phys.* **2003**, *119*, 5740−5761.
(36) Shirts, M. R.; Pande, V. S. Solvation Free Energies of Amino Acid Side Chain Analogs for Common Molecular Mechanics Water Models. *J. Chem. Phys.* **2005**, *122*, 134508.
(37) *The PyMOL Molecular Graphics System*, version 1.5.0.4; Schrdinger, LLC.: New York, 2010.
(38) Duan, Y.; Wu, C.; Chowdhury, S.; Lee, M. C.; Xiong, G.; Zhang, W.; Yang, R.; Cieplak, P.; Luo, R.; Lee, T.; et al. A Point-Charge Force Field for Molecular Mechanics Simulations of Proteins Based on Condensed-Phase Quantum Mechanical Calculations. *J. Comput. Chem.* **2003**, *24*, 1999−2012.
(39) Pronk, S.; Páll, S.; Schulz, R.; Larsson, P.; Bjelkmar, P.; Apostolov, R.; Shirts, M. R.; Smith, J. C.; Kasson, P. M.; van der Spoel, D.; et al. GROMACS 4.5: A High-Throughput and Highly Parallel Open Source Molecular Simulation Toolkit. *Bioinformatics* **2013**, *29*, 845−854.
(40) Hess, B.; Kutzner, C.; van der Spoel, D.; Lindahl, E. GROMACS 4: Algorithms for Highly Efficient, Load-Balanced, and Scalable Molecular Simulation. *J. Chem. Theory Comput.* **2008**, *4*, 435−447.
(41) Berendsen, H. J. C.; Postma, J. P. M.; van Gunsteren, W. F.; DiNola, A.; Haak, J. R. Molecular Dynamics with Coupling to An External Bath. *J. Chem. Phys.* **1984**, *81*, 3684−3690.
(42) Ming, L.-C.; Manghnani, M. H. Isothermal Compression of TiO_2 (Rutile) Under Hydrostatic Pressure to 106 Kbar. *J. Geophys. Res.* **1979**, *84*, 4777−4779.
(43) Hoover, W. G. Canonical Dynamics: Equilibrium Phase-Space Distributions. *Phys. Rev. A: At., Mol., Opt. Phys.* **1985**, *31*, 1695−1697.
(44) Nosé, S. A. Unified Formulation of the Constant Temperature Molecular Dynamics Methods. *J. Chem. Phys.* **1984**, *81*, 511−519.
(45) Essmann, U.; Perera, L.; Berkowitz, M. L.; Darden, T.; Lee, H.; Pedersen, L. G. A Smooth Particle Mesh Ewald Method. *J. Chem. Phys.* **1995**, *103*, 8577−8593.
(46) Darden, T.; York, D.; Pedersen, L. Particle Mesh Ewald: An $N \times \log(N)$ Method for Ewald Sums in Large Systems. *J. Chem. Phys.* **1993**, *98*, 10089−10092.
(47) Fiorin, G.; Klein, M. L.; Hénin, J. Using Collective Variables to Drive Molecular Dynamics Simulations. *Mol. Phys.* **2013**, *111*, 3345−3362.
(48) Tribello, G. A.; Bonomi, M.; Branduardi, D.; Camilloni, C.; Bussi, G. PLUMED 2: New Feathers for an Old Bird. *Comput. Phys. Commun.* **2014**, *185*, 604−613.
(49) Trinquier, G.; Sanejouand, Y. H. Which Effective Property of Amino Acids is Best Preserved by the Genetic Code? *Protein Eng., Des. Sel.* **1998**, *11*, 153−169.
(50) Nawrocki, G.; Cieplak, M. Amino Acids and Proteins at ZnO-Water Interfaces in Molecular Dynamics Simulations. *Phys. Chem. Chem. Phys.* **2013**, *15*, 13628−13636.
(51) Mori, T.; Hamers, R. J.; Pedersen, J. A.; Cui, Q. An Explicit Consideration of Desolvation is Critical to Binding Free Energy Calculations of Charged Molecules at Ionic Surfaces. *J. Chem. Theory Comput.* **2013**, *9*, 5059−5069.
(52) Heinz, H. The Role of Chemistry and pH of Solid Surfaces for Specific Adsorption of Biomolecules in Solution − Accurate

Computational Models and Experiment. *J. Phys.: Condens. Matter* **2014**, *26*, 244105.
(53) Emami, F. S.; Puddu, V.; Berry, R. J.; Varshney, V.; Patwardhan, S. V.; Perry, C. C.; Heinz, H. Force Field and a Surface Model Database for Silica to Simulate Interfacial Properties in Atomic Resolution. *Chem. Mater.* **2014**, *26*, 2647−2658.
(54) Emami, F. S.; Puddu, V.; Berry, R. J.; Varshney, V.; Patwardhan, S. V.; Perry, C. C.; Heinz, H. Prediction of Specific Biomolecule Adsorption on Silica Surfaces as a Function of pH and Particle Size. *Chem. Mater.* **2014**, *26*, 5725−5734.

DOI: 10.1021/acs.jpcc.5b02670
J. Phys. Chem. C 2015, 119, 18126−18139